Effects of deformation and neutron-proton pairing on the Gamow-Teller transitions for ^{24,26}Mg in a deformed quasiparticle random-phase approximation

Eunja Ha* and Myung-Ki Cheoun†
Department of Physics, Soongsil University, Seoul 156-743, Korea
(Received 2 August 2016; revised manuscript received 9 October 2016; published 21 November 2016)

We investigate effects of neutron-proton (np) pairing correlations on the Gamow-Teller (GT) transition of ^{24,26}Mg by explicitly taking into account deformation effects. Our calculation is performed by a deformed quasiparticle random phase approximation (DQRPA) which includes the deformation at the Bardeen-Cooper-Schrieffer and RPA stage. In this paper, we include the np pairing as well as neutron-neutron (nn) and proton-proton (pp) paring correlations to the DQRPA. Our new formalism is applied to the GT transition of well-known deformed Mg isotopes. The np pairing effect is found to affect more or less the GT distribution of ^{24}Mg and ^{26}Mg. But the deformation effect turns out to be much larger than the np paring effect because the Fermi surfaces smear more widely by the deformation rather than the np pairing correlations. Correlations between the deformation and the np pairing effects and their ambiguities are also discussed with the comparison to experimental GT strength data by triton and ^{3}He beams.

DOI: 10.1103/PhysRevC.94.054320

I. INTRODUCTION

Neutron-proton (np) pairing correlations have been thought to play important roles in understanding nuclear structure and related nuclear electromagnetic (EM) and weak transitions for $N = Z$ nuclei [1–6]. In these nuclei, protons and neutrons are usually presumed to occupy the same orbitals and have maximal spatial overlaps. Compared to proton-proton (pp) and neutron-neutron (nn) pairing which have only isovector ($T = 1$), the np pairing correlations have two different modes, viz. isoscalar ($T = 0$) and isovector ($T = 1$). Most studies for the np pairing have focused on $N = Z$ nuclei because the np pairing in the nuclei is expected to be larger than that in $N \neq Z$ nuclei. However, as shown in recent works [7–9], nuclear structure of the $N \neq Z$ nuclei may also be affected by the np pairing correlations.

The importance of the np pairing has been discussed in our early reports for single- and double-β decays [10,11]. But, they were performed by using a spherical quasiparticle random phase approximation (QRPA), which did not include the deformation explicitly. Motivation of the present work is to include the np-pairing effect within a deformed QRPA (DQRPA) approach with a realistic two-body interaction given by the Brueckner G-matrix based on the CD Bonn potential. Therefore, this work is an extension of our previous works for the DQRPA [12,13], in which the deformation effects were consistently treated in the QRPA framework [12], but the np pairing correlations were taken into account only at the Bardeen-Cooper-Schrieffer (BCS) stage [13].

As an application of the DQRPA including the np pairing correlations, we choose GT transitions because the GT strength distributions are sensitive to the nuclear shape and the pairing correlations [14]. For more quantitative comprehension of the np pairing effects and the deformation in the GT transition, we consider two Mg isotopes, ^{24}Mg and ^{26}Mg, which are well-known deformed nuclei and have new systematic GT data by ^{3}He and t beams [15–18]. The np pairing correlations change the conventional quasiparticle concept. The quasineutron and quasiproton concept is to be understood as quasiparticles 1 and 2 which may mix properties of the quasiproton and quasineutron. Therefore, in Sec. II, we explain the DQRPA formalism including all types of pairing correlations as well as the deformation. The applications to the GT transition strength distributions of Mg isotopes are performed in Sec. III with detailed discussions regarding how to determine some parameters inherent in the present formalism. Summary and conclusions are done in Sec. IV.

II. FORMALISM

Theoretical description of the DQRPA approach had been already detailed in our previous paper [12], so that here we briefly summarize the basic formalism. We start from the following nuclear Hamiltonian:

$$
\begin{aligned}
H &= H_0 + H_{\rm int}, \\
H_0 &= \sum_{\rho_\alpha \alpha\alpha'} \epsilon_{\rho_\alpha \alpha\alpha'} c^\dagger_{\rho_\alpha \alpha\alpha'} c_{\rho_\alpha \alpha\alpha'}, \\
H_{\rm int} &= \sum_{\rho_\alpha \rho_\beta \rho_\gamma \rho_\delta, \alpha\beta\gamma\delta, \alpha'\beta'\gamma'\delta'} \\
&\quad \times V_{\rho_\alpha \alpha\alpha' \rho_\beta \beta\beta' \rho_\gamma \gamma\gamma' \rho_\delta \delta\delta'} c^\dagger_{\rho_\alpha \alpha\alpha'} c^\dagger_{\rho_\beta \beta\beta'} c_{\rho_\delta \delta\delta'} c_{\rho_\gamma \gamma\gamma'}, \quad (1)
\end{aligned}
$$

where Greek letters denote proton or neutron single-particle states with a projection Ω of total angular momentum on a nuclear symmetry axis. The projection Ω is treated as the only good quantum number in the deformed basis. $\rho_\alpha (\rho_\alpha = \pm 1)$ denotes a sign of the total angular momentum projection Ω of an α state. Isospin of real particles is denoted by Greek letters with a prime ($\alpha', \beta', \gamma', \delta'$), while isospin of quasiparticles is to be expressed by Greek letters with a double prime. The operator $c^\dagger_{\rho_\alpha \alpha\alpha'}$ ($c_{\rho_\alpha \alpha\alpha'}$) in Eq. (1) stands for a usual creation

*ejha@ssu.ac.kr
†Corresponding author: cheoun@ssu.ac.kr

(destruction) operator of the real particle in a state of $\rho_\alpha\alpha$ with angular momentum projection Ω_α and isospin α'.

A. Deformed BCS equation

The Hamiltonian in Eq. (1) represented by the real particles was then transformed to a quasiparticle representation through Hartree-Fock-Bogoliubov (HFB) transformation,

$$a^\dagger_{\rho_\alpha\alpha\alpha''} = \sum_{\rho_\beta\beta\beta'} (u_{\alpha\alpha''\beta\beta'} c^\dagger_{\rho_\beta\beta\beta'} + v_{\alpha\alpha''\beta\beta'} c_{\rho_\beta\bar\beta\beta'}),$$
$$a_{\rho_\alpha\bar\alpha\alpha''} = \sum_{\rho_\beta\beta\beta'} (u_{\bar\alpha\alpha''\bar\beta\beta'} c_{\rho_\beta\bar\beta\beta'} - v_{\bar\alpha\alpha''\bar\beta\beta'} c^\dagger_{\rho_\beta\beta\beta'}). \quad (2)$$

Since our formalism was intended to include the np pairing correlations, we denoted the isospin of quasiparticles as $\alpha''(\beta'') = 1,2$, while the isospin of real particles was denoted as $\alpha'(\beta') = p,n$. We assumed the time reversal symmetry, which means $u_{\alpha\alpha''\beta\beta'} = u^*_{\bar\beta\alpha''\bar\alpha\beta'}$ and $v_{\alpha\alpha''\beta\beta'} = -v^*_{\bar\beta\alpha''\bar\alpha\beta'}$, and did not allow mixing of different single-particle states (α and β) to the quasiparticle state in a deformed state. However, in a spherical state, the quasiparticle state was mixed with different particle states because each deformed state (basis) can be represented by a linear combination of the spherical state (basis) (see Fig. 1 at Ref. [12]). In this respect, the deformed BCS (DBCS) is another representation of the HFB state in the spherical basis calculation. In actual calculations, we expand all deformed wave functions constructed by a deformed harmonic oscillator basis into the spherical basis, because the Wigner-Eckardt theorem can be only applied to the spherical states and our G matrix was calculated in the spherical basis.

The HFB transformation for each α state was then reduced to the following form:

$$\begin{pmatrix} a^\dagger_1 \\ a^\dagger_2 \\ a_{\bar1} \\ a_{\bar2} \end{pmatrix}_\alpha = \begin{pmatrix} u_{1p} & u_{1n} & v_{1p} & v_{1n} \\ u_{2p} & u_{2n} & v_{2p} & v_{2n} \\ -v_{1p} & -v_{1n} & u_{1p} & u_{1n} \\ -v_{2p} & -v_{2n} & u_{2p} & u_{2n} \end{pmatrix}_\alpha \begin{pmatrix} c^\dagger_p \\ c^\dagger_n \\ c_{\bar p} \\ c_{\bar n} \end{pmatrix}_\alpha \quad (3)$$

and the Hamiltonian could be expressed in terms of the quasiparticle as

$$H' = H'_0 + \sum_{\rho_\alpha\alpha\alpha''} E_{\alpha\alpha''} a^\dagger_{\rho_\alpha\alpha\alpha''} a_{\rho_\alpha\alpha\alpha''} + H_{qp.\mathrm{int}}. \quad (4)$$

Finally, using the transformation of Eq. (3), the following deformed HFB (DHFB) equation was obtained:

$$\begin{pmatrix} \epsilon_p-\lambda_p & 0 & \Delta_{p\bar p} & \Delta_{p\bar n} \\ 0 & \epsilon_n-\lambda_n & \Delta_{n\bar p} & \Delta_{n\bar n} \\ \Delta_{p\bar p} & \Delta_{p\bar n} & -\epsilon_p+\lambda_p & 0 \\ \Delta_{n\bar p} & \Delta_{n\bar n} & 0 & -\epsilon_n+\lambda_n \end{pmatrix}_\alpha \begin{pmatrix} u_{\alpha''p} \\ u_{\alpha''n} \\ v_{\alpha''p} \\ v_{\alpha''n} \end{pmatrix}_\alpha$$
$$= E_{\alpha\alpha''} \begin{pmatrix} u_{\alpha''p} \\ u_{\alpha''n} \\ v_{\alpha''p} \\ v_{\alpha''n} \end{pmatrix}_\alpha, \quad (5)$$

where $E_{\alpha\alpha''}$ is the energy of a quasiparticle with the isospin quantum number α'' in the α state. The pairing potentials in the DHFB Eq. (5) were calculated in the deformed basis by using G matrix calculated from the realistic Bonn CD potential for nucleon-nucleon (NN) interaction as follows:

$$\Delta_{p\bar p\alpha} = \Delta_{\alpha p\bar\alpha p} = -\sum_{J,c} g_{\mathrm{pp}} F^{J0}_{\alpha a\bar\alpha a} F^{J0}_{\gamma c\bar\gamma c} G(aacc,J,T=1) \times (u^*_{1p_c} v_{1p_c} + u^*_{2p_c} v_{2p_c}), \quad (6)$$

$$\Delta_{p\bar n\alpha} = \Delta_{\alpha p\bar\alpha n} = -\sum_{J,c} g_{\mathrm{np}} F^{J0}_{\alpha a\bar\alpha a} F^{J0}_{\gamma c\bar\gamma c} \times \left[G(aacc,J,T=1)\mathrm{Re}\left(u^*_{1n_c} v_{1p_c} + u^*_{2n_c} v_{2p_c}\right) + iG(aacc,J,T=0)\mathrm{Im}\left(u^*_{1n_c} v_{1p_c} + u^*_{2n_c} v_{2p_c}\right)\right], \quad (7)$$

where $F^{JK}_{\alpha a\bar\alpha a} = B^\alpha_a B^\alpha_a (-1)^{j_a-\Omega_\alpha} C^{JK}_{j_a\Omega_\alpha j_a-\Omega_\alpha}(K=\Omega_\alpha-\Omega_\alpha)$ was introduced to represent the G matrix in the deformed basis with the expansion coefficient B_α calculated as [12]

$$B^\alpha_a = \sum_{Nn_z\Sigma} C^{j\Omega_\alpha}_{l\Lambda\frac12\Sigma} A^{N_0 l}_{Nn_z\Lambda} b_{Nn_z\Sigma}, A^{N_0 l n_r}_{Nn_z\Lambda} = \langle N_0 l\Lambda | Nn_z\Lambda\rangle. \quad (8)$$

Here, K, which is a projection number of the total angular momentum J onto the z axis, was selected as $K=0$ at the DHFB stage because we considered pairings of the quasiparticles at α and $\bar\alpha$ states. $G(aaccJ)$ represents a two-body (pairwise) scattering matrix in the spherical basis where all possible scattering of the nucleon pairs inside a nucleus were taken into account.

In the present work, we have included all possible J values, which have $K=0$ projection. $\Delta_{\alpha n\bar\alpha n}$ is calculated in a way similar to Eq. (6) by replacing a proton by a neutron. In order to renormalize the G matrix, strength parameters (g_{pp}, g_{nn}, and g_{np}) were multiplied with the G matrix [10] by adjusting the pairing potentials, $\Delta_{p\bar p}$ and $\Delta_{n\bar n}$, of the lowest state in Eq. (6) to empirical pairing gaps, Δ^{emp}_p and Δ^{emp}_n. The empirical pairing gaps of protons, neutrons, and neutron-proton were evaluated by a symmetric five-term formula for neighboring nuclei [13], for which we exploited empirical masses. Theoretical np pairing gaps were calculated as

$$\delta^{\mathrm{th.}}_{np} = -\left[\left(H^{12}_{\mathrm{g.s.}} + E_1 + E_2\right) - \left(H^{np}_{\mathrm{g.s.}} + E_p + E_n\right)\right]. \quad (9)$$

Here $H^{12}_{\mathrm{g.s.}}$ ($H^{np}_{\mathrm{g.s.}}$) is a total deformed BCS ground state energy with (without) np pairing and E_1+E_2 (E_p+E_n) is a sum of the lowest two quasiparticle energies with (without) np pairing potential Δ_{np} in Eq. (5).

For the mean field energy $\epsilon_{p(n)}$ in Eq. (5), we adopted a deformed Woods-Saxon potential with the universal parameter set [19]. A quadrupole deformation parameter and a hexadecapole deformation parameter, β_2 and β_4, are defined in the following surface radius:

$$R(\theta) = R_0(1 + \beta_2 Y_{20}(\theta) + \beta_4 Y_{40}(\theta)), \quad (10)$$

TABLE I. Deformation parameters and empirical pairing gaps for Mg isotopes.

Nucleus	β_2^{Ours}	β_4^{Ours}	β_2^{E2}	Δ_p^{emp}	Δ_n^{emp}	$\delta_{np}^{\mathrm{emp}}$
^{24}Mg	0.5	0.05	0.605	3.123	3.193	1.844
^{26}Mg	0.5	−0.03	0.482	2.314	1.896	0.143

where the sharp-cut radius $R_0 = 1.2A^{1/3}$ fm [20], and Y_{20} and Y_{40} are spherical harmonics. Table I shows the empirical pairing gaps and the deformation parameter β_2 deduced from the $E2$ transition data with $\beta_2^{\rm ours}$ and $\beta_4^{\rm ours}$ values exploited for Mg isotopes in this work, which are fixed by taking the minimum ground state energy as done in Refs. [21,22]. Detailed calculations for the deformation parameters are presented in Sec. III A.

B. Deformed QRPA equation

Our deformed QRPA (DQRPA) equation was obtained by taking the same approach as the derivation of the QRPA equation in Ref. [23]. But all kinds of pairing correlations are included in the DQRPA. In particular, the np pairing becomes of importance for the description of neutron deficient nuclei, where the Fermi energy of protons may be located near to that of neutrons. This discussion is also addressed in detail in Sec. III. Our DQRPA equation with the np pairing is given by

$$\begin{pmatrix} A^{1111}_{\alpha\beta\gamma\delta}(K) & A^{1122}_{\alpha\beta\gamma\delta}(K) & A^{1112}_{\alpha\beta\gamma\delta}(K) & A^{1121}_{\alpha\beta\gamma\delta}(K) & B^{1111}_{\alpha\beta\gamma\delta}(K) & B^{1122}_{\alpha\beta\gamma\delta}(K) & B^{1112}_{\alpha\beta\gamma\delta}(K) & B^{1121}_{\alpha\beta\gamma\delta}(K) \\ A^{2211}_{\alpha\beta\gamma\delta}(K) & A^{2222}_{\alpha\beta\gamma\delta}(K) & A^{2212}_{\alpha\beta\gamma\delta}(K) & A^{2221}_{\alpha\beta\gamma\delta}(K) & B^{2211}_{\alpha\beta\gamma\delta}(K) & B^{2222}_{\alpha\beta\gamma\delta}(K) & B^{2212}_{\alpha\beta\gamma\delta}(K) & B^{2221}_{\alpha\beta\gamma\delta}(K) \\ A^{1211}_{\alpha\beta\gamma\delta}(K) & A^{1222}_{\alpha\beta\gamma\delta}(K) & A^{1212}_{\alpha\beta\gamma\delta}(K) & A^{1221}_{\alpha\beta\gamma\delta}(K) & B^{1211}_{\alpha\beta\gamma\delta}(K) & B^{1222}_{\alpha\beta\gamma\delta}(K) & B^{1212}_{\alpha\beta\gamma\delta}(K) & B^{1221}_{\alpha\beta\gamma\delta}(K) \\ A^{2111}_{\alpha\beta\gamma\delta}(K) & A^{2122}_{\alpha\beta\gamma\delta}(K) & A^{2112}_{\alpha\beta\gamma\delta}(K) & A^{2121}_{\alpha\beta\gamma\delta}(K) & B^{2111}_{\alpha\beta\gamma\delta}(K) & B^{2122}_{\alpha\beta\gamma\delta}(K) & B^{2112}_{\alpha\beta\gamma\delta}(K) & B^{2121}_{\alpha\beta\gamma\delta}(K) \\ -B^{1111}_{\alpha\beta\gamma\delta}(K) & -B^{1122}_{\alpha\beta\gamma\delta}(K) & -B^{1112}_{\alpha\beta\gamma\delta}(K) & -B^{1121}_{\alpha\beta\gamma\delta}(K) & -A^{1111}_{\alpha\beta\gamma\delta}(K) & -A^{1122}_{\alpha\beta\gamma\delta}(K) & -A^{1112}_{\alpha\beta\gamma\delta}(K) & -A^{1121}_{\alpha\beta\gamma\delta}(K) \\ -B^{2211}_{\alpha\beta\gamma\delta}(K) & -B^{2222}_{\alpha\beta\gamma\delta}(K) & -B^{2212}_{\alpha\beta\gamma\delta}(K) & -B^{2221}_{\alpha\beta\gamma\delta}(K) & -A^{2211}_{\alpha\beta\gamma\delta}(K) & -A^{2222}_{\alpha\beta\gamma\delta}(K) & -A^{2212}_{\alpha\beta\gamma\delta}(K) & -A^{2221}_{\alpha\beta\gamma\delta}(K) \\ -B^{1211}_{\alpha\beta\gamma\delta}(K) & -B^{1222}_{\alpha\beta\gamma\delta}(K) & -B^{1212}_{\alpha\beta\gamma\delta}(K) & -B^{1221}_{\alpha\beta\gamma\delta}(K) & -A^{1211}_{\alpha\beta\gamma\delta}(K) & -A^{1222}_{\alpha\beta\gamma\delta}(K) & -A^{1212}_{\alpha\beta\gamma\delta}(K) & -A^{1221}_{\alpha\beta\gamma\delta}(K) \\ -B^{2111}_{\alpha\beta\gamma\delta}(K) & -B^{2122}_{\alpha\beta\gamma\delta}(K) & -B^{2112}_{\alpha\beta\gamma\delta}(K) & -B^{2121}_{\alpha\beta\gamma\delta}(K) & -A^{2111}_{\alpha\beta\gamma\delta}(K) & -A^{2122}_{\alpha\beta\gamma\delta}(K) & -A^{2112}_{\alpha\beta\gamma\delta}(K) & -A^{2121}_{\alpha\beta\gamma\delta}(K) \end{pmatrix} \times \begin{pmatrix} \tilde{X}^m_{(\gamma1\delta1)K} \\ \tilde{X}^m_{(\gamma2\delta2)K} \\ \tilde{X}^m_{(\gamma1\delta2)K} \\ \tilde{X}^m_{(\gamma2\delta1)K} \\ \tilde{Y}^m_{(\gamma1\delta1)K} \\ \tilde{Y}^m_{(\gamma2\delta2)K} \\ \tilde{Y}^m_{(\gamma1\delta2)K} \\ \tilde{Y}^m_{(\gamma2\delta1)K} \end{pmatrix} = \hbar\Omega^m_K \begin{pmatrix} \tilde{X}^m_{(\alpha1\beta1)K} \\ \tilde{X}^m_{(\alpha2\beta2)K} \\ \tilde{X}^m_{(\alpha1\beta2)K} \\ \tilde{X}^m_{(\alpha2\beta1)K} \\ \tilde{Y}^m_{(\alpha1\beta1)K} \\ \tilde{Y}^m_{(\alpha2\beta2)K} \\ \tilde{Y}^m_{(\alpha1\beta2)K} \\ \tilde{Y}^m_{(\alpha2\beta1)K} \end{pmatrix}, \tag{11}$$

where 1 and 2 mean isospins of quasiparticles denoted as $\alpha''(\beta'')$ in previous sections. The amplitudes $\tilde{X}^m_{(\alpha\alpha''\beta\beta'')K}$ and $\tilde{Y}^m_{(\alpha\alpha''\beta\beta'')K}$ stand for forward and backward going amplitudes from state $\alpha\alpha''$ to $\beta\beta''$.

Our DQRPA equation has a very general form because we include the deformation as well as all kinds of pairing correlations still remaining in the mean field. If we switch off the np pairing, all off-diagonal terms in the A and B matrices of the left hand side of Eq. (11) disappear with the replacement of 1 and 2 with p and n. Then the DQRPA equation is decoupled into $pp + nn + pn + np$ DQRPA equations. For charge conserving (or neutral current) reactions, $pp + nn$ DQRPA can describe the $M1$ spin or EM transitions on the same nuclear species, while $np + pn$ DQRPA describes the GT$(-/+)$ transitions in the charge exchange (or charged current) reactions. Also it should be noted that the np DQRPA is different from the pn DQRPA because of the deformation. But, if we neglect the np pairing, i.e., take only 1212 terms and $\alpha\beta\gamma\delta = (pnp'n')$ in the matrices, quasiparticles 1 and 2 reduce to quasiproton and quasineutron, and Eq. (11) becomes the np DQRPA at Ref. [24]. One more point to be noticed is that, if we use the spherical QRPA, this equation is reduced to the QRPA equation in Ref. [10].

The A and B matrices in Eq. (11) are given by

$$\begin{aligned} A^{\alpha''\beta''\gamma''\delta''}_{\alpha\beta\gamma\delta}(K) &= (E_{\alpha\alpha''} + E_{\beta\beta''})\delta_{\alpha\gamma}\delta_{\alpha''\gamma''}\delta_{\beta\delta}\delta_{\beta''\delta''} - \sigma_{\alpha\alpha''\beta\beta''}\sigma_{\gamma\gamma''\delta\delta''} \\ &\times \sum_{\alpha'\beta'\gamma'\delta'} [-g_{pp}(u_{\alpha\alpha''\alpha'}u_{\beta\beta''\beta'}u_{\gamma\gamma''\gamma'}u_{\delta\delta''\delta'} + v_{\alpha\alpha''\alpha'}v_{\beta\beta''\beta'}v_{\gamma\gamma''\gamma'}v_{\delta\delta''\delta'})V_{\alpha\alpha'\beta\beta',\gamma\gamma'\delta\delta'} \\ &- g_{\rm ph}(u_{\alpha\alpha''\alpha'}v_{\beta\beta''\beta'}u_{\gamma\gamma''\gamma'}v_{\delta\delta''\delta'} + v_{\alpha\alpha''\alpha'}u_{\beta\beta''\beta'}v_{\gamma\gamma''\gamma'}u_{\delta\delta''\delta'})V_{\alpha\alpha'\delta\delta',\gamma\gamma'\beta\beta'} \\ &- g_{\rm ph}(u_{\alpha\alpha''\alpha'}v_{\beta\beta''\beta'}v_{\gamma\gamma''\gamma'}u_{\delta\delta''\delta'} + v_{\alpha\alpha''\alpha'}u_{\beta\beta''\beta'}u_{\gamma\gamma''\gamma'}v_{\delta\delta''\delta'})V_{\alpha\alpha'\gamma\gamma',\delta\delta'\beta\beta'}], \end{aligned} \tag{12}$$

$$\begin{aligned} B^{\alpha''\beta''\gamma''\delta''}_{\alpha\beta\gamma\delta}(K) &= -\sigma_{\alpha\alpha''\beta\beta''}\sigma_{\gamma\gamma''\delta\delta''} \sum_{\alpha'\beta'\gamma'\delta'} [g_{pp}(u_{\alpha\alpha''\alpha'}u_{\beta\beta''\beta'}v_{\gamma\gamma''\gamma'}v_{\delta\delta''\delta'} + v_{\alpha\alpha''\alpha'}v_{\bar{\beta}\beta''\beta'}u_{\gamma\gamma''\gamma'}u_{\bar{\delta}\delta''\delta'})V_{\alpha\alpha'\beta\beta',\gamma\gamma'\delta\delta'} \\ &- g_{\rm ph}(u_{\alpha\alpha''\alpha'}v_{\beta\beta''\beta'}v_{\gamma\gamma''\gamma'}u_{\delta\delta''\delta'} + v_{\alpha\alpha''\alpha'}u_{\beta\beta''\beta'}u_{\gamma\gamma''\gamma'}v_{\delta\delta''\delta'})V_{\alpha\alpha'\delta\delta',\gamma\gamma'\beta\beta'} \\ &- g_{\rm ph}(u_{\alpha\alpha''\alpha'}v_{\beta\beta''\beta'}u_{\gamma\gamma''\gamma'}v_{\delta\delta''\delta'} + v_{\alpha\alpha''\alpha'}u_{\beta\beta''\beta'}v_{\gamma\gamma''\gamma'}u_{\delta\delta''\delta'})V_{\alpha\alpha'\gamma\gamma',\delta\delta'\beta\beta'}], \end{aligned} \tag{13}$$

where u and v coefficients are determined from the DBCS calculation with the pairing strength parameters $g^{n}_{\rm pair}, g^{p}_{\rm pair}$, and $g^{np}_{\rm pair}$ adjusted to the empirical pairing gaps Δ_{nn}, Δ_{pp}, and δ_{np}, respectively. $E_{\alpha\alpha''}$ indicates the quasiparticle energy of the state α with the quasiparticle isospin $\alpha'' = 1$ or 2. The two-body interactions $V_{\alpha\beta,\gamma\delta}$ and $V_{\alpha\delta,\gamma\beta}$ are particle-particle and particle-hole matrix elements of the residual NN interaction V, respectively, in the deformed state calculated by the G matrix. Detailed manipulations were explained in Ref. [12].

The $\beta^{\pm}$ decay operator, $\hat{\beta}^{\pm}_{1\mu}$, is defined in an intrinsic frame as

$$\hat{\beta}^{-}_{1\mu} = \sum_{\alpha\beta} \langle \alpha p | \tau^{+} \sigma_K | \beta n \rangle c^{\dagger}_{\alpha p} \tilde{c}_{\beta n}, \quad \hat{\beta}^{+}_{1\mu} = (\hat{\beta}^{-}_{1\mu})^{\dagger} = (-)^{\mu} \hat{\beta}^{-}_{1,-\mu}. \tag{14}$$

The $\beta^{\pm}$ transition amplitudes from the ground state of an initial (parent) nucleus to an excited state of a daughter nucleus, i.e., one phonon state K^{+} in a final nucleus, are written as

$$\begin{aligned}
\langle K^{+}, m | \hat{\beta}^{-}_{K} | \mathrm{DQRPA} \rangle &= \sum_{\alpha\alpha''\rho_\alpha\beta\beta''\rho_\beta} \mathcal{N}_{\alpha\alpha''\rho_\alpha\beta\beta''\rho_\beta} \langle \alpha\alpha'' p \rho_\alpha | \sigma_K | \beta\beta'' n \rho_\beta \rangle \left[u_{\alpha\alpha'' p} v_{\beta\beta'' n} X^{m}_{(\alpha\alpha''\beta\beta'')K} + v_{\alpha\alpha'' p} u_{\beta\beta'' n} Y^{m}_{(\alpha\alpha''\beta\beta'')K} \right], \\
\langle K^{+}, m | \hat{\beta}^{+}_{K} | \mathrm{DQRPA} \rangle &= \sum_{\alpha\alpha''\rho_\alpha\beta\beta''\rho_\beta} \mathcal{N}_{\alpha\alpha''\beta\beta''} \langle \alpha\alpha'' p \rho_\alpha | \sigma_K | \beta\beta'' n \rho_\beta \rangle \left[u_{\alpha\alpha'' p} v_{\beta\beta'' n} Y^{m}_{(\alpha\alpha''\beta\beta'')K} + v_{\alpha\alpha'' p} u_{\beta\beta'' n} X^{m}_{(\alpha\alpha''\beta\beta'')K} \right],
\end{aligned} \tag{15}$$

where $|\mathrm{DQRPA}\rangle$ denotes a correlated DQRPA ground state in the intrinsic frame and the normalization factor is given as $\mathcal{N}_{\alpha\alpha''\beta\beta''}(J) = \sqrt{1 - \delta_{\alpha\beta}\delta_{\alpha''\beta''}(-1)^{J+T}}/(1 + \delta_{\alpha\beta}\delta_{\alpha''\beta''})$. The forward and backward amplitudes, $X^{m}_{(\alpha\alpha''\beta\beta'')K}$ and $Y^{m}_{(\alpha\alpha''\beta\beta'')K}$, are related to $\tilde{X^{m}}_{(\alpha\alpha''\beta\beta'')K} = \sqrt{2}\sigma_{\alpha\alpha''\beta\beta''} X^{m}_{(\alpha\alpha''\beta\beta'')K}$ and $\tilde{Y^{m}}_{(\alpha\alpha''\beta\beta'')K} = \sqrt{2}\sigma_{\alpha\alpha''\beta\beta''} Y^{m}_{(\alpha\alpha''\beta\beta'')K}$ in Eq. (11), where $\sigma_{\alpha\alpha''\beta\beta''} = 1$ if $\alpha = \beta$ and $\alpha'' = \beta''$, otherwise $\sigma_{\alpha\alpha''\beta\beta''} = \sqrt{2}$ [10].

III. RESULTS AND DISCUSSIONS

A. Deformation and shell evolution

This study exploited a cylindrical Woods-Saxon potential for the mean field with the universal parameter set in Ref. [19]. Particle model space for Mg isotopes was exploited up to $N = 5\hbar\omega$ for a deformed basis and up to $N = 10\hbar\omega$ for a spherical basis. In our previous paper [25], single particle states obtained from the deformed Woods-Saxon potential were shown to be sensitive to a deformation parameter β_2. Therefore we determined the β_2 value by minimizing a ground state energy, which is a sum of a deformed mean field energy calculated by the Woods-Saxon potential and a pairing energy evaluated at the DBCS stage. But pairing energy contributions to the ground state energy turns out to be much smaller than those by the mean field as shown in Fig. 1, in which pairing strengths for np, nn, and pp are determined for each β_2 value to fit empirical pairing gaps deduced from standard mass tables.

In Fig. 1, total ground state energies for ^{24,26}Mg, $E_{\rm tot} = E_{\rm MF'} + E_{\rm pair}$, are presented as a sum of the deformed Woods-Saxon mean field energy and the pairing energy by the BCS calculations, as a function of the quadrupole deformation parameter β_2. $E_{\rm MF'}$ (black squares) denotes a total energy of the quasiparticles in the mean field calculated with respectd to the Fermi surface and $E_{\rm pair}$ (blue triangles) is a sum of all pairing energies of the quasiparticles. The lowest total energy is $-232.18(-266.16)$ MeV at $\beta_2 = 0.6(0.5)$ for ^{24}Mg(^{26}Mg). The β_2 values are quite consistent with those extracted from $E2$ transition data, 0.605(0.482) for ^{24}Mg (^{26}Mg). One remarkable point is that spherical shape nuclei favor larger (deeper) pairing energies, while oblate or prolate nuclear shapes favor smaller (shallower) pairing energy. This stems from the fact that single particle states are widely scattered by the deformation, which weakens the overlap of nucleon wave functions for the pairing correlations.

Next, we switch on the hexadecapole deformation parameter β_4 which was assumed to be $0 \sim \pm 0.05$ in this calculation. In Fig. 2, total energies are shown in terms of the deformation parameter β_2 and β_4 in the deformed Woods-Saxon potential. The lowest ground state energy is obtained as $-233.06(-266.82)$ MeV with $\beta_2 = 0.5$ and $\beta_4 = 0.05$ ($\beta_2 = 0.5$ and $\beta_4 = -0.03$), respectively, for ^{24}Mg(^{26}Mg). Although these β_2 values are a bit different from those obtained in Fig. 1, we use these β_2 and β_4 values hereafter. All of the values for the parameters used in this calculation are recapitulated in Table I. In the last subsection, Sec. III C, we discussed possible ambiguities coming from the uncertainty of the deformation parameter β_2 to be deduced in Fig. 2.

Before the analysis of GT($-/+$) strength distributions for ^{24,26}Mg, in Fig. 3, we show a shell evolution of neutron single particle state energies (SPSE) in ^{26}Mg along with the β_2 value. One may easily notice that the deformation is a key ingredient for the shell evolution. Specifically, the $0d5/2$ state is split into three different states by the deformation, which makes other submagic numbers, 10 and 12, for the $\beta_2 = 0.5$ case. For example, the $5/2^{+}_{1}(3/2^{+}_{2})$ state in the Nilsson basis stems from the $0d5/2(0d3/2)$ state in spherical basis and gives rise to the submagic number in the deformed basis. Here J^{π}_{i} [or $J(i)\pi$ in the legend] means the ith state of each single particle state (SPS) having a spin J and parity π.

One important point to be noticed is that, by the $\beta_2 \sim 0.5$ deformation, an energy gap between two main shells, $1s1/2$ and $0d5/2$ states holding 14 neutrons, in the spherical shape disappears and a new energy gap is generated in the deformed shape above $3/2^{+}_{1}$ state keeping 12 neutrons. Therefore, the open shell structure of $^{24}_{12}\mathrm{Mg}_{12}$ in the spherical shape changes to a closed shell structure, so that repulsive particle-hole (p-h) interaction in the GT transition [26] becomes dominant and pushes the GT excitation to a bit higher excitations. On the contrary, for $^{26}_{12}\mathrm{Mg}_{14}$, the closed shell structure becomes an

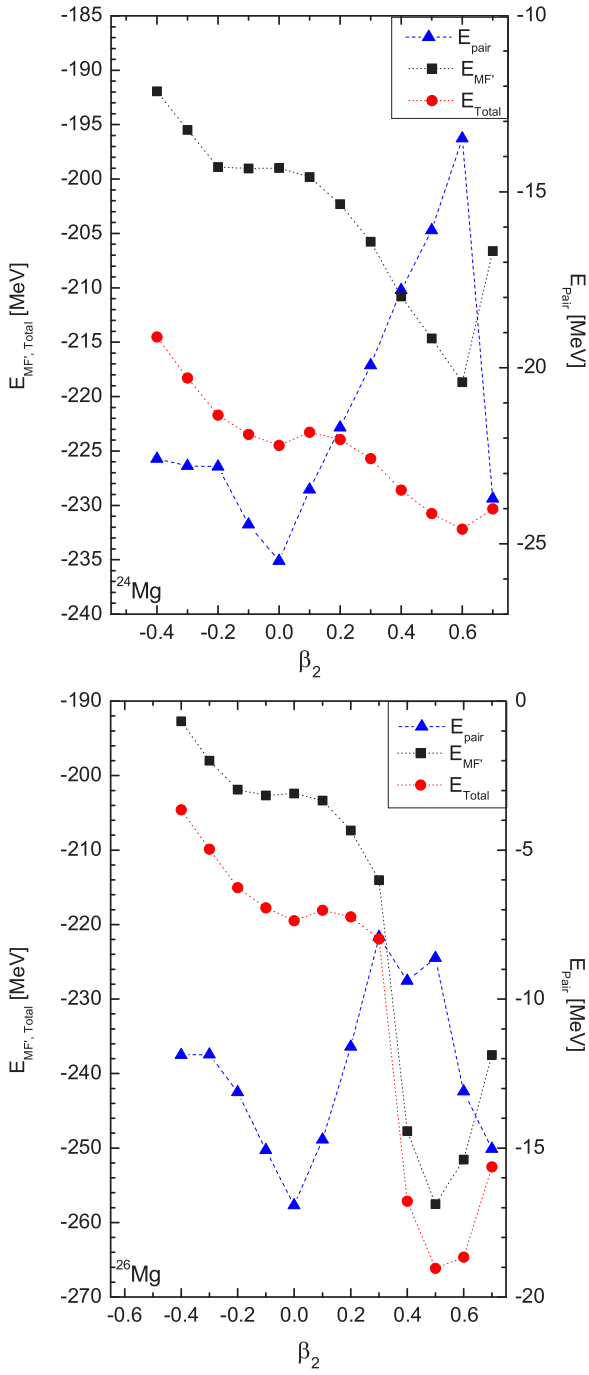

FIG. 1. Total ground state energies of ^{24,26}Mg, $E_{\rm tot} = E_{\rm MF'} + E_{\rm Pair}$ for different β_2 values. They are calculated by a sum of the deformed WS mean field energy ($E_{\rm MF}$) and the pairing energy ($E_{\rm pair}$). $E_{\rm MF'}$ and $E_{\rm tot}$ are presented with respect to the Fermi surface energy. Marking of $E_{\rm pair}$ are shown in the right y label. Here we neglected the contribution by the β_4 deformation because it is much smaller than that by the β_2 variation.

open shell structure by the deformation, which leads to a mixture of attractive particle-particle (p-p) and repulsive p-h interaction and scatters widely the GT strength distribution. These features are confirmed in the experimental GT($-$) data as discussed in Sec. III C.

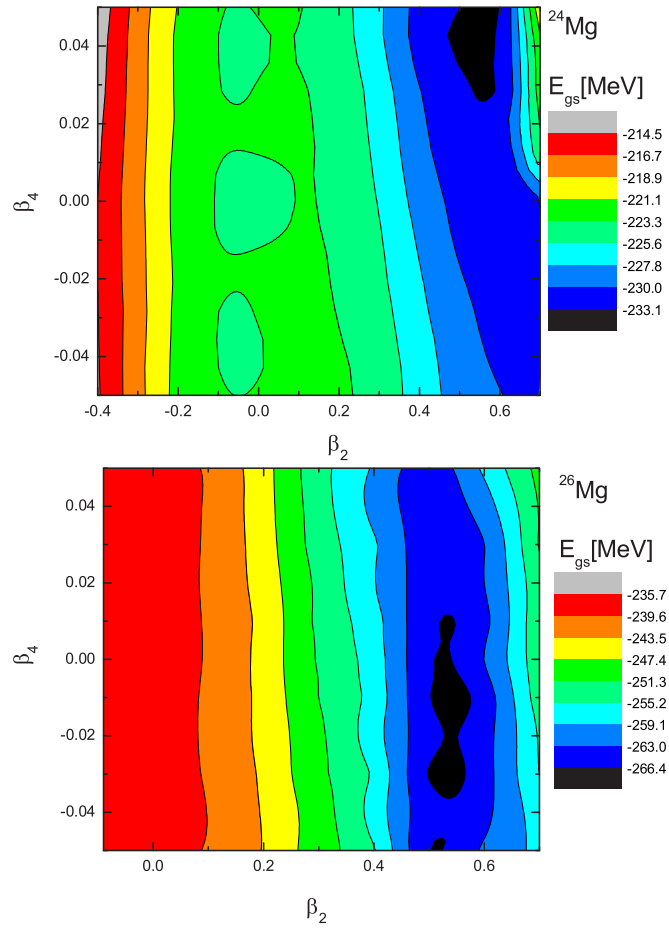

FIG. 2. Contours of total ground state energies of ^{24,26}Mg as a function of β_2 and β_4 deformations.

B. GT($-$/+) transitions for ^{24}Mg

Figure 4 shows our numerical results of the GT($-$) strength distribution, B(GT($-$)), for ^{24}Mg. Deformation effects in panels (d) and (e) by the β_2 and β_4 deformation scatter

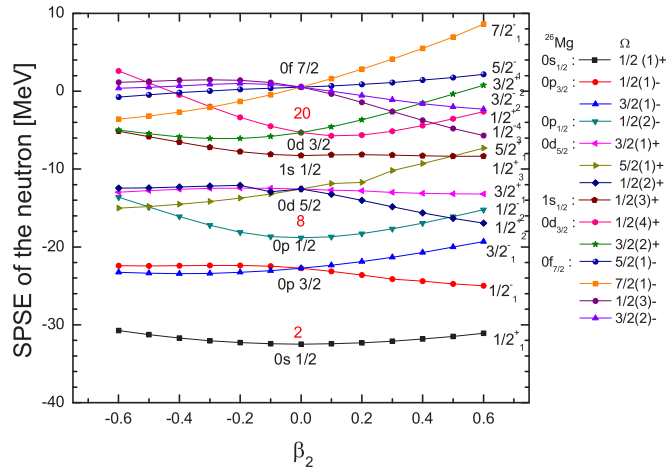

FIG. 3. Evolution of neutron single-particle state energies (SPSE) for ^{26}Mg as a function of β_2 deformation.

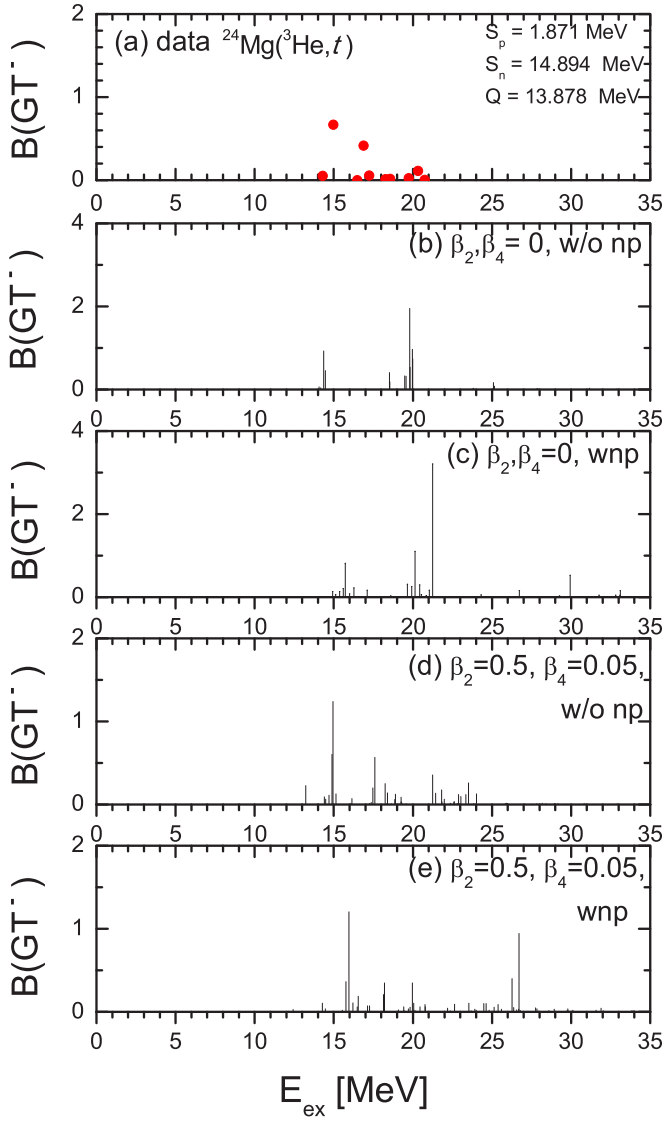

FIG. 4. Gamow-Teller [GT(−)] transition strength distribution B(GT(−)) of ^{24}Mg. Experimental data by ^{3}He beam in (a) are from Ref. [16]. Results of (b) and (c) are the spherical case, i.e., $\beta_2, \beta_4 = 0$ with and without the np pairing. (d) and (e) are the case of the $\beta_2 = 0.5, \beta_4 = 0.05$ cases with and without the np pairing. Our results are presented by the excitation energy from the parent nucleus. Here the error of the GT data is reported as about 10%.

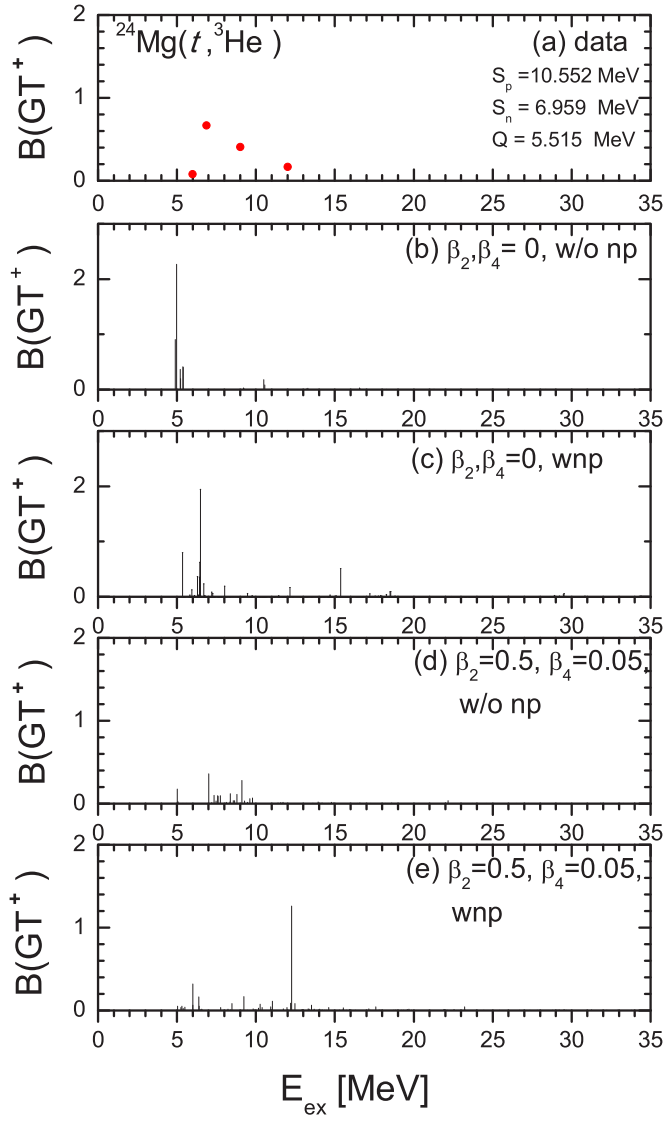

FIG. 5. The same as Fig. 4, but for B(GT(+)) of ^{24}Mg. Experimental data by t beam in (a) are from Ref. [15]. Here the error of the GT data is reported as about 5%.

reasonably two main peak strengths in spherical shape [panels (b) and (c)] to a wider, but relatively higher, excitation energy region with general attenuation. This behavior comes from the repulsive p-h interaction in the closed shell structure evolved from the spherical shape by the deformation. Our results are presented by taking a 0.1 MeV bin in DQRPA excitation energy.

In high-lying GT states, the np pairing effects become significant compared to those in low-lying states. In particular, as shown in (c) and (e) of Fig. 4, some GT strengths appear at the higher excitation energy region around 30 MeV and 27 MeV region by attractive np pairing force. It can be understood from the fact that the attractive np pairing reduces the Fermi energy gap of neutrons and protons, $\Delta\epsilon^F = |\epsilon_n^F - \epsilon_p^F|$, by which the neutrons below Fermi surface may more easily transit to proton states.

Both deformation and np pairing effects also showed up in the GT(+) case in Fig. 5. The deformation scatters and weakens the peak strength around 5 MeV region and the np pairing predicts some GT(+) contributions above 15 MeV and 12 MeV region [see panels (c) and (e) of Fig. 5.]. These high-lying excited states expected in the GT(−/+) transition due to the np pairing correlations could affect thermal nuclear reactions in the cosmos as well as the g_A quenching problem inside nuclei. For more intuitive and systematic understanding the GT(−/+) strength, we present GT running sums with experimental data in Fig. 6. Here we used the universal quenching factor 0.79, which is a bit larger than that used in Zegers [16].

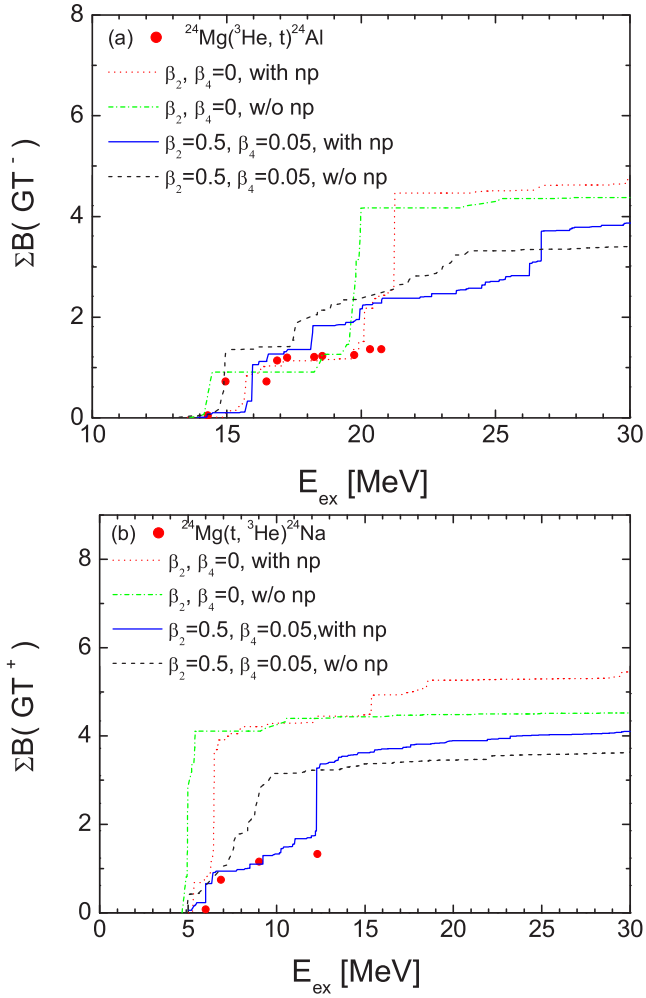

FIG. 6. Running sums for the GT (−/+) strength distributions (a)–(e) in Figs. 4 and 5. Results by Zegers *et al.* are experimental data deduced from Refs. [16] and [15].

C. GT(−/+) transitions for ^{26}Mg

Numerical results for GT(−/+) transitions and their running sums in ^{26}Mg are given in Figs. 7–9. Deformation strongly influences GT(−/+) transitions. It scatters and largely attenuates a peak around 13 MeV for the GT(−) and 7 MeV for the GT(+) transition in spherical shape. But the *np* pairing effects for ^{26}Mg are not more significant than those for the ^{24}Mg case. It means that, once the deformation is included, the smearing of the Fermi surface by the *np* pairing is not so large as the smearing by the deformation. In the experimental data of Fig. 7, we can notice lots of GT(−) states which come from the shell evolution to an open shell by the deformation, as explained Sec. III A and Fig. 3. But one may notice that theoretical strength of the first GT excited state at 4.99 MeV is still deficient, and the fourth peak at 8.77 MeV is a bit large compared to experimental data, as shown in panels (d) and (e) of Fig. 7. Also the GT(+) strengths in Figs. 8 and 9 are not good enough to explain the data.

In Fig. 10, we analyze the first and the fourth GT(−) peaks in Fig. 7. Main configurations of the four GT(−) excited states ($E_{\rm ex}$ = 4.99, 8.77, 11.21, and 14.65 MeV) are ($\pi 5/2^+_1$, $\nu 5/2^+_1$)

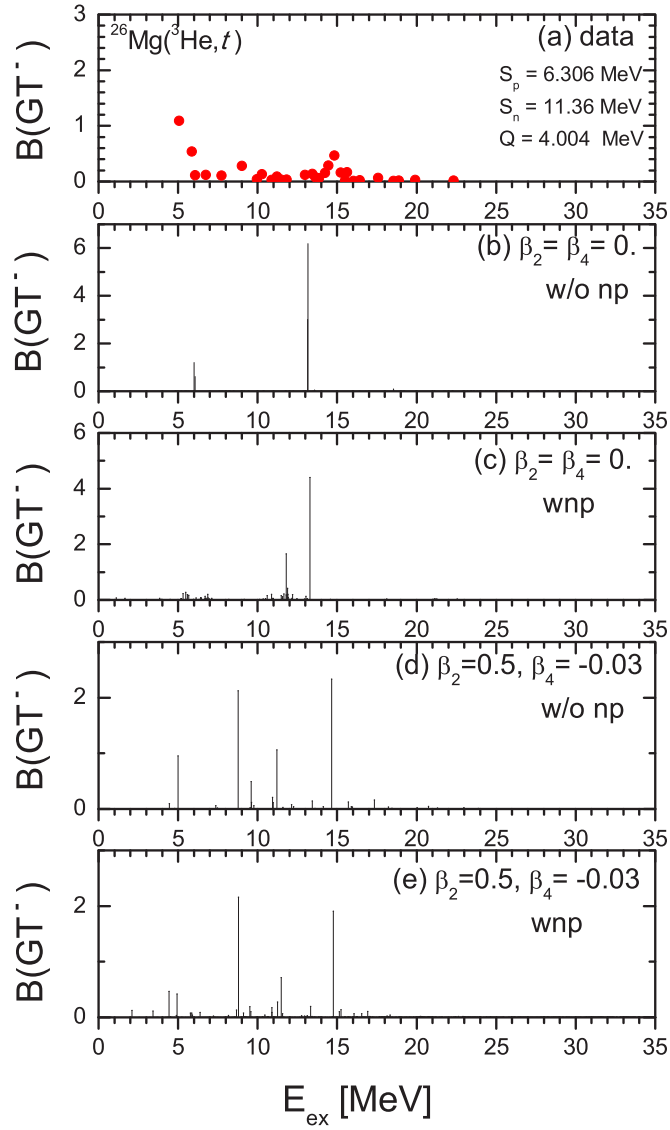

FIG. 7. Gamow-Teller (GT−) transition strength distribution B(GT(−)) of ^{26}Mg. Experimental data by ^{3}He beam in (a) are from Ref. [18]. Results of (b) and (c) are the spherical case with and without the *np* pairing, i.e., $\beta_2, \beta_4 = 0$. (d) and (e) are the case of the $\beta_2 = 0.5, \beta_2 = -0.03$ case with and without the *np* pairing. Our results are presented by the excitation energy from the parent nucleus.

(black line), ($\pi 1/2^+_3$, $\nu 3/2^+_1$) (red line), ($\pi 1/2^+_3$, $\nu 1/2^+_2$) (green line), and ($\pi 3/2^+_2$, $\nu 5/2^+_1$) (blue line), respectively. Occupation amplitudes for each SPS in the configurations are also presented in the figure.

According to Eq. (15), the main factors for the GT(−) excitation are $v_n u_p$, single particle matrix element $\langle \alpha\alpha'' p\rho_\alpha | \sigma_K | \beta\beta'' n\rho_\beta \rangle$ and X forward amplitude. Since the $v_n u_p$ factors are nearly equal to each other (see black and blue lines for the first and fourth peak), a key ingredient is the single particle matrix element, $\langle p5/2^+_1 | \sigma_K | n5/2^+_1 \rangle$ and $\langle p1/2^+_3 | \sigma_K | n1/2^+_3 \rangle$ (second largest configuration) for the firstt and $\langle p3/2^+_2 | \sigma_K | n5/2^+_1 \rangle$ for the fourth peak. But the $K = 1$ transition for the fourth peak is enumerated as almost two times larger than the $K = 0$ transitions in the first peak. This is the

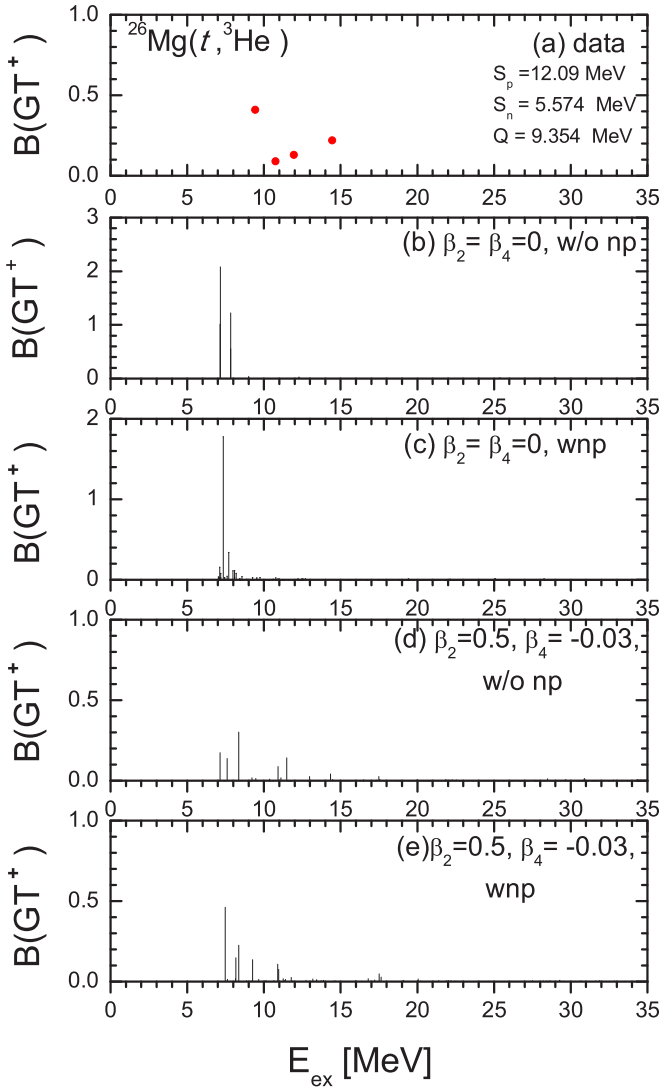

FIG. 8. The same as in Fig. 7, but for B(GT(+)) of ^{26}Mg.

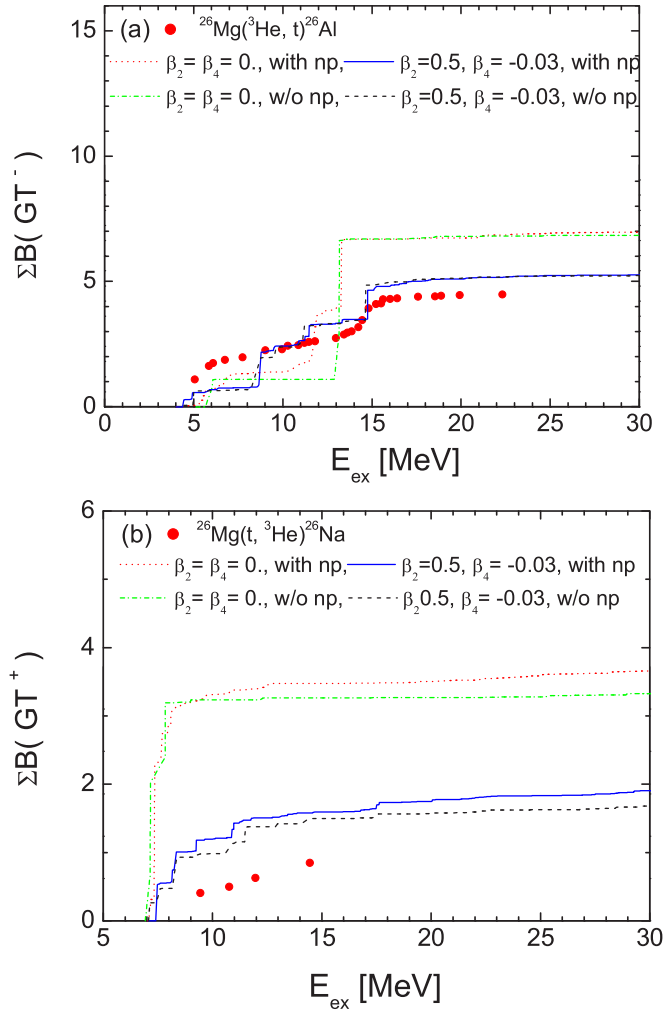

FIG. 9. Running sums for the GT (−) strength distributions (a)–(e) in Figs. 7 and 8. Results by Zegers *et al.* are experimental data deduced from Ref. [18].

reason why we have relatively larger peak around 15 MeV region. More detailed analyses are necessary for further understanding these peak strengths because the occupation probabilities largely depend on the nuclear model. For GT(+) transition, as shown in Fig. 8, a peak position at 9 MeV is also not properly reproduced enough even if the deformation and the *np* pairings are taken into account. This behavior is also thought to come from the mixture of the *p-h* and *p-p* residual interaction due to the open shell property by the deformation in ^{26}Mg. Running sums for both GT(−/+) strengths are presented in Fig. 9, which show more or less reasonable behavior compatible to the data. But there are still remained some disagreements with the GT data, which may result from the uncertainties associated with the parameters for the DQRPA. These points are discussed in the next subsection.

D. Uncertainties and ambiguities in the DQRPA

It is well known that the quasiparticle concept does not guarantee the exact particle number at BCS and RPA stages. In the BCS, one may usually constrain average particle numbers by using the Lagrangian multiplier (or chemical potential). But, at the RPA stage, there are no ways to conserve particle numbers of the QRPA excited state. In this paper, correction of the particle number nonconservation peculiar to the QRPA approach is done by the following way [27,28]. In principle, the excitation energy is given as

$$E_{\rm ex} = \langle\Psi_{\rm ex}|H' + \lambda_n\hat{N} + \lambda_p\hat{Z}|\Psi_{\rm ex}\rangle - \langle\Psi_{\rm gr}|H' + \lambda_n\hat{N} + \lambda_p\hat{Z}|\Psi_{\rm gr}\rangle, \quad (16)$$

where $H' = H - \lambda_n\hat{N} - \lambda_p\hat{Z}$ is the system Hamiltonian including chemical potentials as Lagrangian multipliers for the particle conservation, and $|\Psi_{\rm ex}\rangle$ and $|\Psi_{\rm gr}\rangle$ are the DQRPA excited and DBCS ground states, respectively. In the QRPA scheme, $\langle\Psi_{\rm ex}|H'|\Psi_{\rm ex}\rangle - \langle\Psi_{\rm gr}|H'|\Psi_{\rm gr}\rangle$ in Eq. (16) is usually approximated as $\hbar\Omega$ without considering the terms relevant to the chemical potentials. In this work, corrections of the DQRPA excitation energies to the particle number deviation

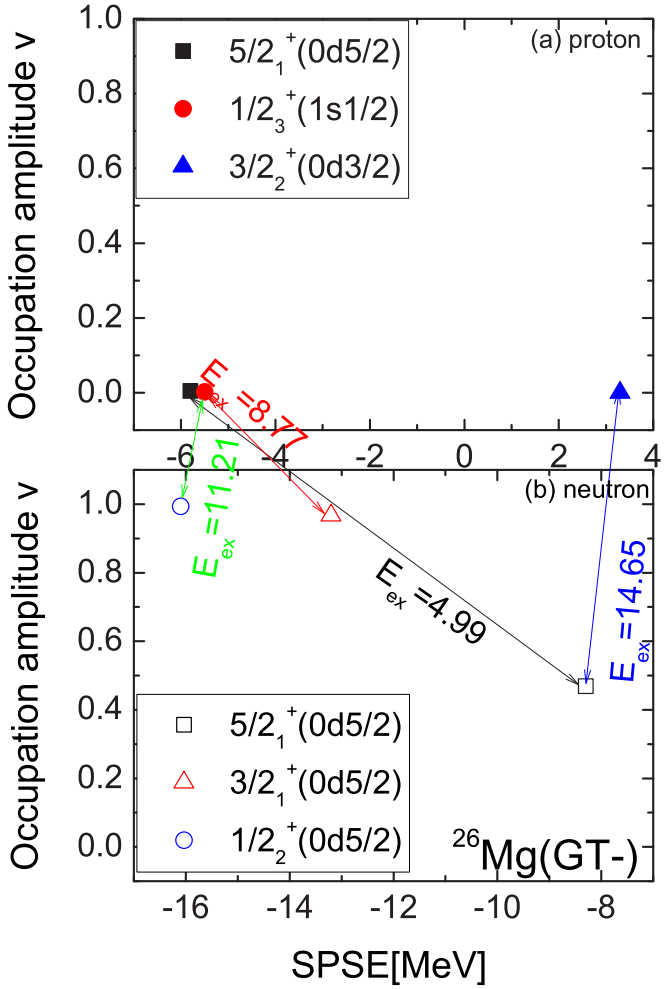

FIG. 10. Occupation amplitudes (v) of protons and neutrons as a function of the SPSE for the four main GT($-$) peaks for ^{26}Mg at $E_{ex} = 4.99$ MeV (black line), 8.77 MeV (red line), 11.21 MeV (green line), and 14.65 MeV (blue line) in Fig. 7(d). Filled (empty) symbols denote the occupation amplitudes of proton (neutron).

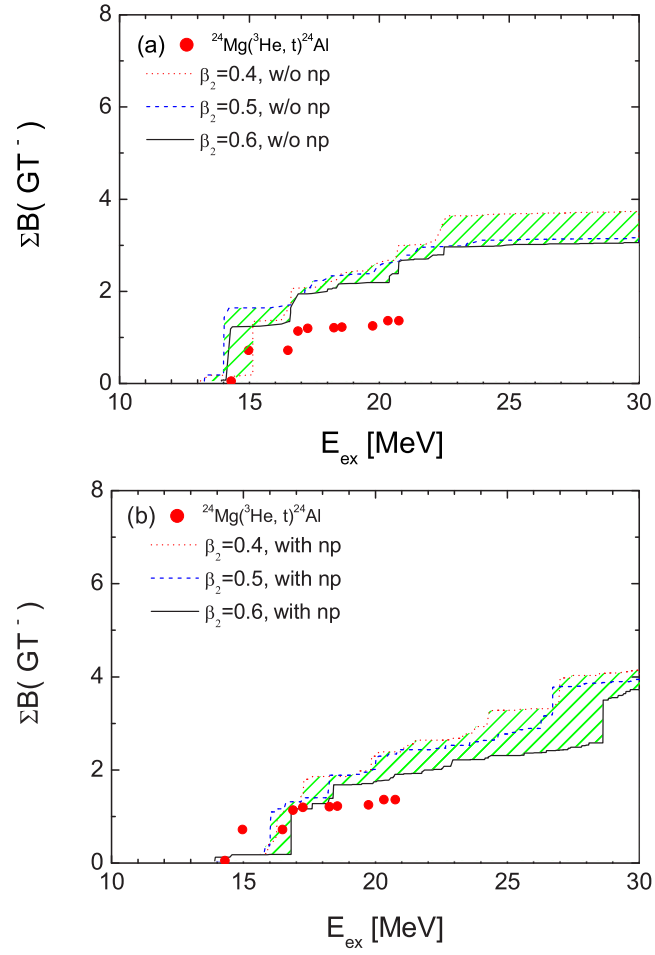

FIG. 11. Error analysis for the deformation parameter $\beta_2 = 0.4 \sim 0.6$ for ^{24}Mg in running sums for GT ($-$) strength distributions. (a) and (b) are the results without and with the np pairing correlations. Experimental data are deduced from Ref. [16]. Dashed area are results obtained by allowing $\beta_2 = 0.5 \pm 0.1$.

have been done by explicitly including the terms as follows:

$$E_{\rm ex}^{\rm QRPA} = \hbar\Omega + \langle\Psi_{\rm ex}|\lambda_n\hat{N} + \lambda_p\hat{Z}|\Psi_{\rm ex}\rangle - \langle\Psi_{\rm gr}|\lambda_n\hat{N} + \lambda_p\hat{Z}|\Psi_{\rm gr}\rangle. \quad (17)$$

We approximate the last two terms as $\langle\Psi_{\rm ex}|\hat{N}|\Psi_{\rm ex}\rangle = N \mp 1, \langle\Psi_{\rm ex}|\hat{Z}|\Psi_{\rm ex}\rangle = Z \pm 1, \langle\Psi_{\rm gr}|\hat{N}|\Psi_{\rm gr}\rangle = N, \langle\Psi_{\rm gr}|\hat{Z}|\Psi_{\rm gr}\rangle = Z$ for GT($-/+$) transitions. All of the results in this work are corrected by Eq. (17). In fact, this correction is the same approach as adopted in Ref. [29], which includes the particle number correction in the QRPA equation.

As for the deformation parameter β_2, although we deduced it as 0.5 for ^{24,26}Mg from Fig. 2, we have still some errors of the order 0.1 as shown in the figure. In Fig. 11, we performed error estimation by the uncertainty of β_2. It has been done for the running sum of the GT($-$) strength distribution, Σ(B(GT($-$)), for ^{24}Mg. Dashed area bands in panels (a) and (b) represent accumulative GT strengths without and with the np pairing, respectively. Low-lying GT strength results with the np become compatible with the data. But they still overestimate data, which needs a smaller quenching factor than used in this work.

Finally, we address the ambiguity coming from the np pairing correlations. In fact, there are many discussions regarding how to include the np pairing at the BCS stage [7–9]. Here we adopted a conventional approach, namely, a unified BCS theory [3], where we take pairing correlations between a state and its time conjugated state, i.e., $p\bar{p}$, $n\bar{n}$, $p\bar{n}$, and $n\bar{p}$. But there is a more general BCS scheme, the isospin-generalized BCS theory, which takes into account the pn pairing leading to a 8×8 unitary transformation. The empirical pairing gaps can also be refined if we take more neighboring nuclei into account. In the present work, the GT strength results including the np pairing correlations may become sometimes worse than those by without the np pairing. More refined data and general theoretical approaches for the np pairing correlations are necessary for further definite evidence of the np pairing correlations.

IV. SUMMARY AND CONCLUSION

In summary, we added the neutron-proton (np) pairing correlations, which have spin-triplet and isospin-singlet ($J = 1, T = 0$), and spin-singlet and isospin-triplet ($J = 0, T = 1$) component, to a proton-neutron DQRPA by explicitly exploiting the G matrix for the nucleon-nucleon interaction inside nuclei. Our approach was applied to the Gamow-Teller transitions for $N = Z$ and $N \neq Z$ nuclei of Mg isotopes, ^{24,26}Mg.

The pairing correlations including the np pairing were found to be strongly and systematically correlated to the deformation of ^{24,26}Mg. The stronger deformation reduces contributions of the pairing energy. The attractive np pairing effects manifest themselves in high-lying GT states due to the reduction of Fermi energy gap of protons and neutrons. It means that the np pairing correlations may influence on the nuclear structure of $N \sim Z$ light nuclei as well as medium or heavy nuclei, if Fermi energies of the neutron and proton are adjacent to each other. But, for deformed nuclei such as Mg isotopes considered in the present work, main effect in the GT transition turns out to come from the deformation. These phenomena are also inferred from the modified smearing of the Fermi surface mainly due to the shell evolution by the deformation effect.

For example, ^{24}Mg would have an open sd-shell structure in its spherical shape. But, by the deformation, the open shell evolves to a closed shell as shown in Fig. 3. Then the repulsive particle-hole (p-h) interaction shifts the GT excitation to a bit higher excitation states. On the contrary, ^{26}Mg evolves to its open shell characteristics by the deformation. As a result, mixing of the repulsive particle-hole and the attractive particle-particle force makes the GT excitations more complicated than ^{24}Mg. In this case, one needs to develop more refined theoretical descriptions rather than the present DQRPA, such as renormalized DQRPA and continuum DQRPA. But they are beyond the scope of the present work.

In conclusion, it turns out that the np pairing effects as well as the deformation effects can be important not only for medium and heavy $N \sim Z$ nuclei but also for light $N \sim Z$ nuclei. But more refined and general approaches for the np pairing at the BCS stage are necessary for further conclusions. Nevertheless, these effects may affect many important nuclear electromagnetic and weak transitions in nuclear astrophysics as well as nuclear physics. Extension of the present approach to medium heavy nuclei, in particular, the mass region considerably treated in the nuclear astrophysics, are in progress.

ACKNOWLEDGMENTS

This work was supported by the National Research Foundation of Korea (Grant Nos. NRF-2015R1D1A4A01020477, NRF-2014R1A2A2A05003548). We would like to acknowledge the support from KISTI supercomputing center for computing time and the MPI parallelization.

[1] H. T. Chen and A. Goswami, Phys. Lett. B **24**, 257 (1967).
[2] H. H. Wolter, A. Faessler, and P. U. Sauer, Phys. Lett. B **31**, 516 (1970).
[3] A. L. Goodman, Phys. Rev. C **58**, R3051 (1998); **60**, 014311 (1999).
[4] J. Engel, S. Pittel, M. Stoitsov, P. Vogel, and J. Dukelsky, Phys. Rev. C **55**, 1781 (1997).
[5] O. Civitarese, M. Reboiro, and P. Vogel, Phys. Rev. C **56**, 1840 (1997).
[6] F. Simkovic, Ch. C. Moustakidis, L. Pacearescu, and A. Faessler, Phys. Rev. C **68**, 054319 (2003).
[7] Alexandros Gezerlis, G. F. Bertsch, and Y. L. Luo, Phys. Rev. Lett. **106**, 252502 (2011).
[8] W. A. Friedman and G. F. Bertsch, Eur. Phys. J. A **41**, 109 (2009).
[9] B. A. Brown, Phys. Rev. Lett. **111**, 162502 (2013).
[10] M. K. Cheoun, A. Bobyk, A. Faessler, F. Simkovic, and G. Teneva, Nucl. Phys. A **561**, 74 (1993); **564**, 329 (1993); M. K. Cheoun, A. Faessler, F. Šimkovic, G. Teneva, and A. Bobyk, *ibid.* **587**, 301 (1995).
[11] G. Pantis, F. Simkovic, J. D. Vergados, and A. Faessler, Phys. Rev. C **53**, 695 (1996).
[12] Eunja Ha and Myung-Ki Cheoun, Nucl. Phys. A **934**, 73 (2015).
[13] Eunja Ha, Myung-Ki Cheoun, and F. Simkovic, Phys. Rev. C **92**, 044315 (2015).
[14] P. Sarriguren, E. Moya de Guerra, and A. Escuderos, Nucl. Phys. A **658**, 13 (1999).
[15] M. E. Howard *et al.*, Phys. Rev. C **78**, 047302 (2008).
[16] R. G. T. Zegers *et al.*, Phys. Rev. C **78**, 014314 (2008).
[17] R. Madey *et al.*, Phys. Rev. C **35**, 2011 (1987).
[18] R. G. T. Zegers *et al.*, Phys. Rev. C **74**, 024309 (2006).
[19] S. Cwiok *et al.*, Comput. Phys. Commun. **46**, 379 (1987).
[20] P. Ring, Y. K. Gambhir, and G. A. Lalazissis, Comput. Phys. Commun. **105**, 77 (1997).
[21] P. Sarriguren, E. Moya de Guerra, L. Pacearescu, Amand Faessler, F. Simkovic, and A. A. Raduta, Phys. Rev. C **67**, 044313 (2003).
[22] P. Sarriguren and J. Pereira, Phys. Rev. C **81**, 064314 (2010); P. Sarriguren, A. Algora, and J. Pereira, *ibid.* **89**, 034311 (2014).
[23] Jouni Suhonen, *From Nucleons to Nucleus* (Springer-Verlag, Berlin/Heidelberg, 2007).
[24] M. S. Yousef, V. Rodin, A. Faessler, and F. Simkovic, Phys. Rev. C **79**, 014314 (2009).
[25] Eunja Ha and Myung-Ki Cheoun, Phys. Rev. C **88**, 017603 (2013).
[26] Y. Fujita, B. Rubio, and W. Gelletly, Prog. Part. Nucl. Phys. **66**, 549 (2011).
[27] R. A. Eramzhyan, V. A. Kuz'min, and T. V. Tetereva, Nucl. Phys. A **643**, 428 (1998).
[28] Eunja Ha, Myung-Ki Cheoun, and K. S. Kim, J. Korean Phys. Soc. **67**, 1142 (2015).
[29] O. Civitarese, H. Muther, L. D. Skouras, and Amand Faessler, J. Phys. G **17**, 1363 (1991).